JOURNAL OF SOLID STATE CHEMISTRY **131,** 94–100 (1997)
ARTICLE NO. SC977349

Electric and Magnetic Properties of $LiMn_2O_4$- and Li_2MnO_3-Type Oxides

V. Massarotti, D. Capsoni, M. Bini, and G. Chiodelli

Dipartimento di Chimica Fisica e CSTE-CNR, Universita' degli Studi di Pavia, via Taramelli 16, I-27100 Pavia, Italy

C. B. Azzoni and M. C. Mozzati

Istituto Nazionale di Fisica della Materia, Dipartimento di Fisica ''Alessandro Volta,'' Universita' degli Studi di Pavia, via Bassi 6, I-27100 Pavia, Italy

and

A. Paleari

Istituto Nazionale di Fisica della Materia, Dipartimento di Fisica, Universita' degli Studi di Milano, via Celoria 16, I-20133 Milano, Italy

Received October 21, 1996; in revised form February 7, 1997; accepted February 14, 1997

XRD measurements proved the coexistence of spinel, lithium-rich spinel, and rock-salt phases in the Li–Mn–O system. An investigation of the electrical properties, carried out on polycrystalline samples, shows that Li_2MnO_3 has insulating behavior while the spinel phases provide an example of hopping conduction mechanism. The negative Seebeck coefficient suggests that electrons constitute the charge carriers and their number is consistent with the fraction of Mn^{3+} over the total number of Mn^{3+} and Mn^{4+} sites in the spinel structure. The static magnetic susceptibility results agree with the presence of the Mn^{3+} ions in high spin configuration.

1. INTRODUCTION

The compounds of the Li–Mn–O system are studied for both theoretical and practical interest. The spinel $LiMn_2O_4$ and related phases possess peculiar applications in the fields of electrochemistry (1–4) and catalysis (5–7).

Starting from the reactive system MnO/Li_2CO_3, the formation of $LiMn_2O_4$ (stoichiometric lithium cationic fraction $x = 0.33$) was recently studied and evidence was found of both stoichiometric and nonstoichiometric (Li-rich) spinel phases in $x > 0.35$ samples (8, 9). Recent data are now available on composition-related defects involving Li^+ ions from both structural-calorimetric (10) and structural-spectroscopic (11) studies.

In the spinel phase, Mn^{4+} and Mn^{3+} ions are present and deviations from stoichiometry were detected, with the resulting composition $Li[Li_yMn_{2-y}]O_4$. In the stoichiometric spinel ($y = 0$) a cubic–tetragonal transition occurs at about 280 K (10) and was attributed to cooperative Jahn–Teller distortion around the Mn^{3+} cation sites. Moreover, very low deviations from the exact stoichiometry ($0 < y < 0.04$) remarkably lower both the temperature and the enthalpy of the transition. As it can be inferred, structural analysis, magnetic susceptibility, mass magnetization, and transport measurements can be powerful tools to show how a lithium excess gives rise to Li substitution for Mn in the spinel cationic site, with an increase in Mn^{4+} (and decrease in Mn^{3+}) ion fraction in the same lattice site. For higher lithium excess, a further cubic spinel phase, with a significantly different lattice parameter, was considered (8, 9), where Li substitution for Mn in the octahedral (16*d*) site *W* as assumed.

The aim of the present work was to investigate structural, transport, and magnetic properties of these lithium/manganese compounds and to relate them to the bulk composition and to the coexistence of two distinct valence states of Mn cations, whose fractions could be tuned by changing the lithium content.

The knowledge of such relationships should be extremely useful in the stage of selection and preparation of electrode materials.

2. EXPERIMENTAL

2.1. Materials and Sample Preparation

The samples were prepared by the reactive system Alfa (99.9%) MnO/Carlo Erba (R.P.) Li_2CO_3 from a starting mixture with a lithium cationic fraction, *x*, ranging between 0.33 and 0.53. Each mixture was fired in air for 8 h at 1073 K

0022-4596/97 $25.00

and for 8 h at 1173 K. Both heating and cooling rates were 5 K/min. Pure Li_2MnO_3 was obtained from a $x = 0.667$ reactive mixture subjected to the thermal treatment just described.

Powder samples for electrochemical characterization were pressed in to the forms of disks and bars, and then they were sintered for 12 h at 1173 K in air.

2.2. Apparatus and Procedures

Diffraction data were obtained by a Philips PW1710 powder diffractometer equipped with a Philips PW1050 vertical goniometer. Cu$K\alpha$ radiation ($K\alpha_1 = 1.54056$ Å; $K\alpha_2 = 1.5443$ Å) was used by means of a graphite monochromator. Patterns were collected in the angular range $15^\circ < 2\theta < 130^\circ$ in step scan mode.

The Rietveld refinement procedure (12) performed with the programs WYRIET version 3.5 (13) and DBWS3.2S (14) was used to obtain the abundance and stoichiometry of the phases (8, 9, 15). A more accurate peak profile refinement was performed by using the LS1 program (16), taking into account microstructural (crystallite size and microstrain) parameters, using an annealed sample of BaF_2 as a suitable standard for the determination of the instrumental line broadening parameters.

Four-electrode dc resistivity measurements were performed by using a Solartron 1286 galvanostat/electrometer apparatus. To evaluate the microstructural contribution to the resistivity of the samples, the impedance spectroscopy technique was applied and a Solartron 1255 or 1260 frequency response analyzer (FRA) was used in the frequency range 10^{-3} to 10^7 Hz, with a homemade high-impedance adaptor ($10^{12}\,\Omega$, 3 pF) (17). A Leybold ROK10 cryostat was used for low-temperature electrical measurements. The thermoelectric power (α) and oxygen transport number (t_i) measurements were performed by means of the electrochemical cell described elsewhere (18). The electromotive force at the two opposite electrodes was measured as a function of the increasing thermal gradient (for the α data) and of the oxygen partial pressure difference (for the t_i data).

Static magnetic susceptibility measurements were carried out from 300 to 77 K at a magnetic field of 200 mT by using a Faraday balance susceptometer with a sensitivity of 0.1 μg and a continuous-flow cryogenic apparatus. For sample masses of a few 10^{-2} g, the resulting sensitivity is about $10^{-7}\,cm^3/g$. The error on the absolute mass susceptibility data, derived from the accuracy in the magnetic-field gradient value, is estimated to be less than 10%. The magnetic-field dependence of the magnetization was also monitored at different temperatures by changing the field intensity between 50 and 450 mT.

3. RESULTS

3.1. XRD Results

The XRD patterns of the $LiMn_2O_4$ ($x = 0.33$) and Li_2MnO_3 ($x = 0.67$) samples display the expected lines. The synthesis of spinel with intermediate compositions gives rise to samples which show a Li-rich spinel phase, in addition to $LiMn_2O_4$ and Li_2MnO_3 (8–10). Thus three phases were included in the structural model for the Rietveld profile refinement with the objective of determining the abundance and composition of the phases. The results are summarized in Table 1. The final comparison between experimental and calculated patterns for the $x = 0.40$ sample is reported in Fig. 1. For samples with $x \geq 0.44$ rather large values of the discrepancy factors were obtained in the conventional Rietveld profile analysis (9), due to the anisotropy of the microstructural parameters. To obtain more reliable profile refinement fit, in the present work we take into account suitable microstructural variable parameters in the LS1 program. For the spinel phase the crystallite size components $M_{11} = M_{22} = M_{33}$ and $M_{12} = M_{13} = M_{23}$ and the microstrain components $\varepsilon_{11} = \varepsilon_{22} = \varepsilon_{33}$ and

TABLE 1
Stoichiometry and Percentages of the Phases

x	0.33	0.35	0.36	0.38	0.40	0.44	0.53	0.67
Stoichiom. spinel		$Li_{1.06}Mn_{1.94}O_4$						
$LiMn_2O_4$								
%	100	99.5	49	41	40	47	25	0
Li-rich spinel								
$Li_{1+y}Mn_{2-y}O_4$								
y			0.17	0.12	0.19	0.27	0.22	
%	0	0	49	52	52	31	20	0
Rock salt								
Li_2MnO_3								
%	0	0.5	2	7	8	22	55	100

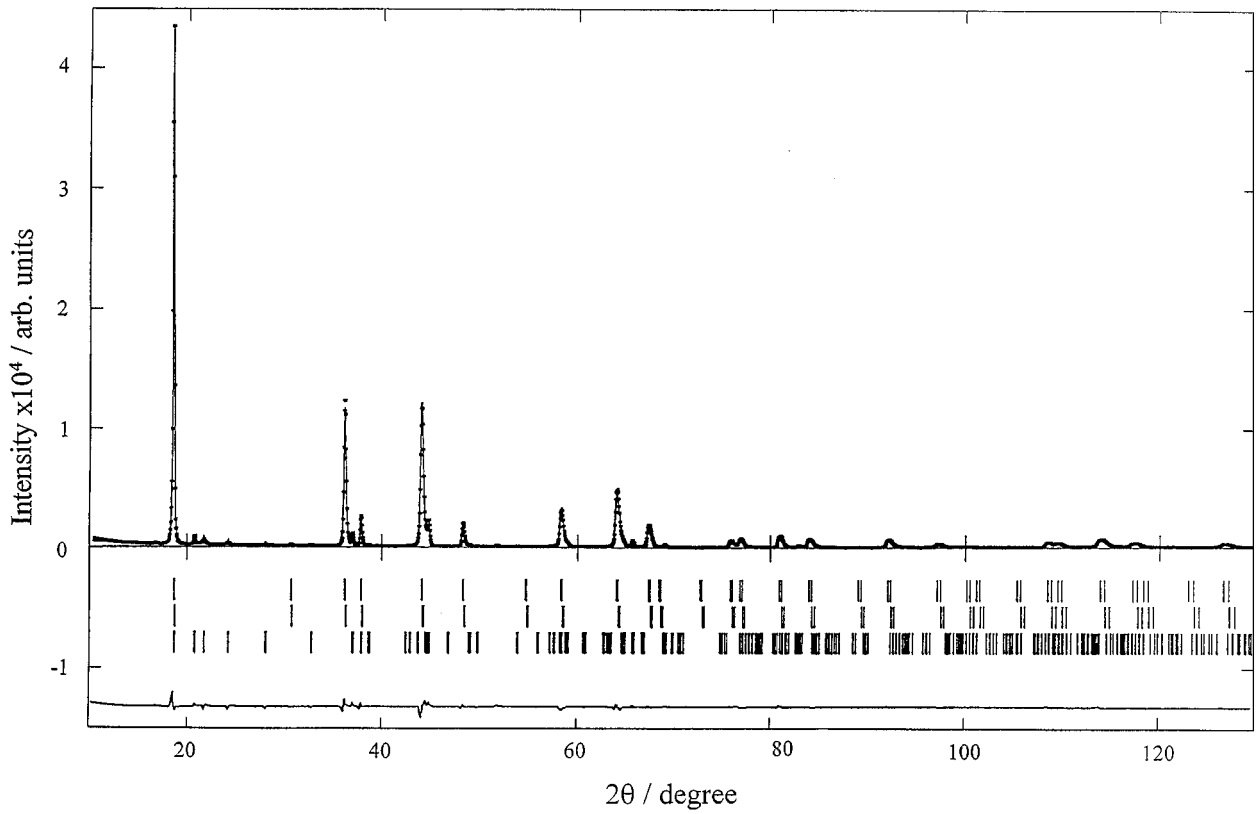

FIG. 1. Comparison between observed (dots) and calculated (solid line) X-ray profile after refinement for the $x = 0.40$ sample. In the lower part the difference is plotted: the bars (from the top) represent the reflection positions of stoichiometric $LiMn_2O_4$ spinel, Li-rich spinel, and Li_2MnO_3 coexisting phases.

$\varepsilon_{12} = \varepsilon_{13} = \varepsilon_{23}$ were used, while for the rock-salt phase the independent components were M_{11}, M_{22}, M_{33} and M_{12} ($M_{13} = M_{23} = 0$) and ε_{11}, ε_{22}, ε_{33} and ε_{12} ($\varepsilon_{13} = \varepsilon_{23} = 0$). The pertinent refinement results are summarized in Table 2. The marked anisotropic behavior of both samples, consistent with the wide range of variation of the microstructural parameters, can explain the more satisfactory agreement between the experimental FWHM values (Fig. 2, closed circles) and the values calculated with the LS1 program (open lozenges), in comparison with the values calculated by the conventional Rietveld profile analysis, i.e., without consideration of any microstructural influence (solid line).

3.2. *Conductivity Results*

The results of the conductivity measurements are summarized in the Arrhenius plot and in the complex impedance plot of Fig. 3, while the isothermal conductivity plots, as a function of Li content, are shown in Fig. 4. In Fig. 3a the comparison between the present data (continuous line) and the literature data (closed circles) (21) is also shown for the $x = 0.33$ sample.

As observed in these figures, the conductivity is practically independent of the composition in the range $0.33 < x < 0.40$, while for $x > 0.40$ it decreases assuming a different thermal behavior. The pure monoclinic compound

TABLE 2
Crystallite Size and Microstrain Parameters

Sample	Crystallite size (Å)				Microstrain ($\Delta d/d$)			
	M_{11}	M_{22}	M_{33}	M_{12}	ε_{11}	ε_{22}	ε_{33}	ε_{12}
Spinel	6.3×10^2	6.3×10^2	6.3×10^2	1.0×10^3	1.3×10^{-3}	1.3×10^{-3}	1.3×10^{-3}	1.0×10^{-6}
Rock-salt	3.3×10^2	7.0×10^2	1.2×10^3	$\cong 0$	1.0×10^{-6}	9.5×10^{-4}	5.0×10^{-4}	1.0×10^{-6}

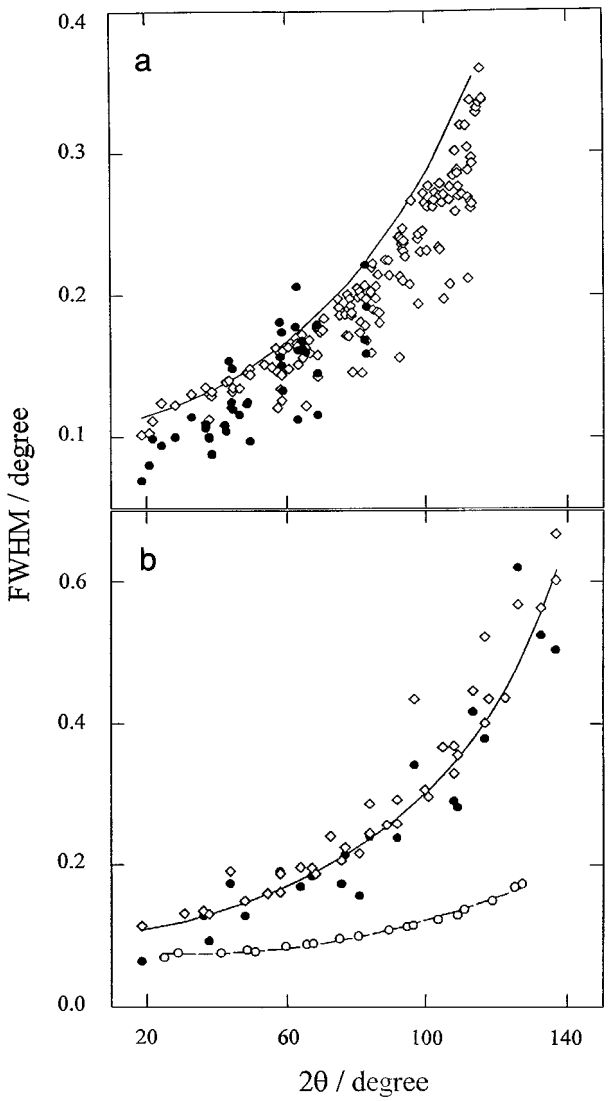

FIG. 2. FWHM dependence on the diffraction angle of (a) $x = 0.667$ Li_2MnO_3 peaks (●) and (b) $x = 0.33$ $LiMn_2O_4$ peaks (●) compared with the FWHM from Rietveld refinement (solid line) and the FWHM obtained taking into account microstructural effects (◇). In (b) the FWHM of the BaF_2 standard peaks (○) with a parabolic interpolation (dashed line) is also reported.

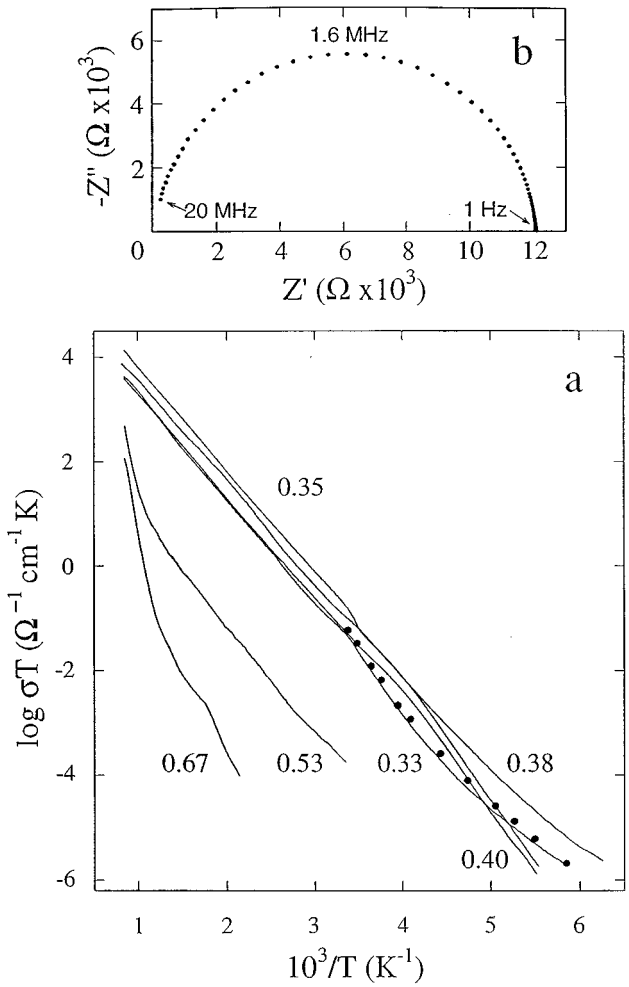

FIG. 3. (a) Arrhenius plot deduced from conductivity measurements on different composition samples (solid lines) are compared with literature data (●) (21). (b) Impedance plot of $LiMn_2O_4$ at room temperature.

($x = 0.67$) can be considered substantially an insulating phase. An activation energy value of 0.40 eV can be determined for the conduction process in the samples with $0.33 < x < 0.40$ in the 100–1000 K range.

Impedance spectroscopy measurements, showing a single half circle covering the entire frequency range (Fig. 3b) for the $x = 0.33$ sample, indicate that the resistivity values obtained by the four-probe dc technique must be attributed to bulk properties, so excluding grain-boundary contribution. The frequency-independent impedance data in the low-frequency range, as a consequence of the absence of relaxation phenomena attributed to electrode reaction, including oxygen and lithium ions, reproduce a quite common feature of electronically conducting materials. Indeed, the ionic transport number measurements, performed at room temperature with an oxygen partial pressure gradient, give a null value of the oxygen contribution to the total conduction.

The spinel conductivity data reported in Fig. 5a show a sensible variation between 283 and 287 K and similar behavior is observable from the magnetic susceptibility measurements as shown in Fig. 5b.

The thermopower data are reported in Fig. 6 for the conducting samples with $x = 0.33$, $x = 0.38$, and $x = 0.40$ and are compared with the values obtained by Schutte *et al.* (21) for a stoichiometric spinel sample. The Seebeck coefficient α is negative and nearly independent of the composition and of the temperature in the wide 290–1073 K range.

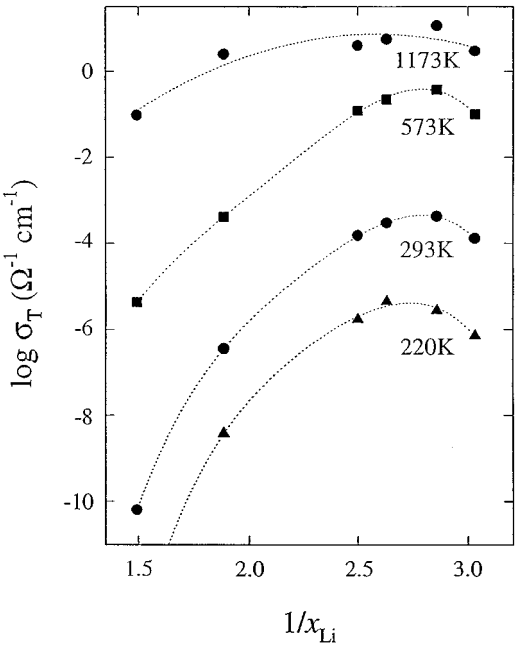

FIG. 4. Isothermal composition dependence of conductivity. The dashed lines are a guide for the eye.

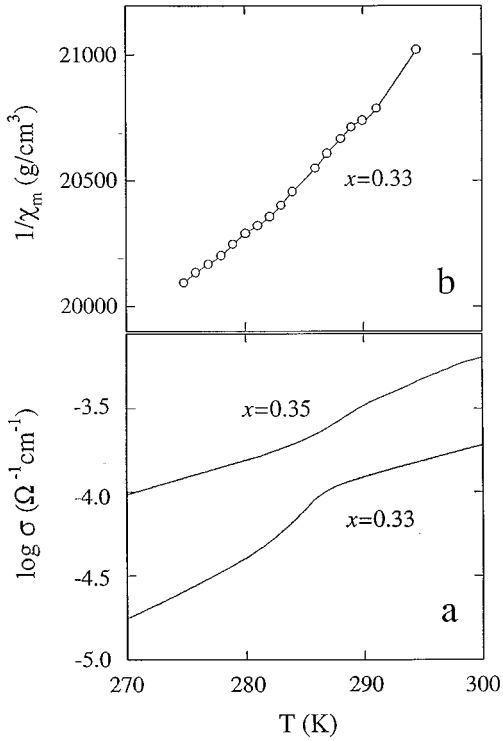

FIG. 5. Temperature dependence close to room temperature in nearly stoichiometric samples. (a) Conductivity data. (b) χ_m^{-1} data.

3.3. Static Magnetic Susceptibility Results

The mass susceptibility (χ_m) data in the range 77–300 K show $1/\chi_m(T)$ behavior substantially linear with negative intercepts (Fig. 7). In fact, the data are well fitted by the Curie–Weiss law

$$1/\chi_m = (T-\theta)/C_m,$$

where C_m is the Curie constant and θ is the Weiss constant.

The magnetic moment per Mn ion is related to the experimental data by the relation

$$m_{exp}^2 = 3kC_mM/(nN_A),$$

where k is the Boltmann constant, N_A is Avogadro's number, M is the molecular weight, and n is the number of Mn ions per unit formula. The m_{exp}, in μ_B (Bohr magneton) units, and θ values deduced from the experimental data are reported in Table 3.

4. DISCUSSION

The negative Seebeck coefficients indicate that the charge carriers are electrons. The $\alpha(T)$ behavior and the low activation energy (0.4 eV) suggest that the transport process is likely due to a thermally activated hopping mechanism. In this case the thermopower may be written as (22)

$$\alpha = \frac{k}{e}\left(\ln\frac{1-c}{c}\beta + \frac{S_T}{k}\right). \qquad [1]$$

In [1] e is the electron charge, c is the ratio n_e/N, n_e and N being the number of sites with one conduction electron and of available hopping sites, respectively, and β is a degeneracy factor of the electronic carriers. The vibrational

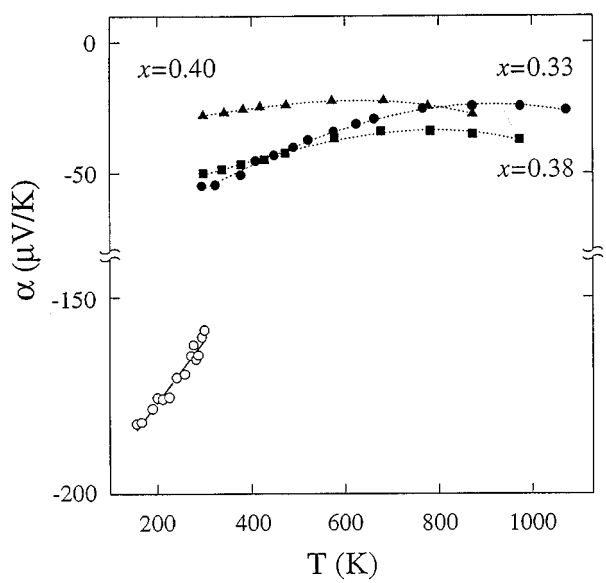

FIG. 6. Temperature dependence of the Seebeck coefficient for the $x = 0.33$, $x = 0.38$, and $x = 0.40$ samples. The low-temperature data (○) from Ref. (21) for a spinel sample are given.

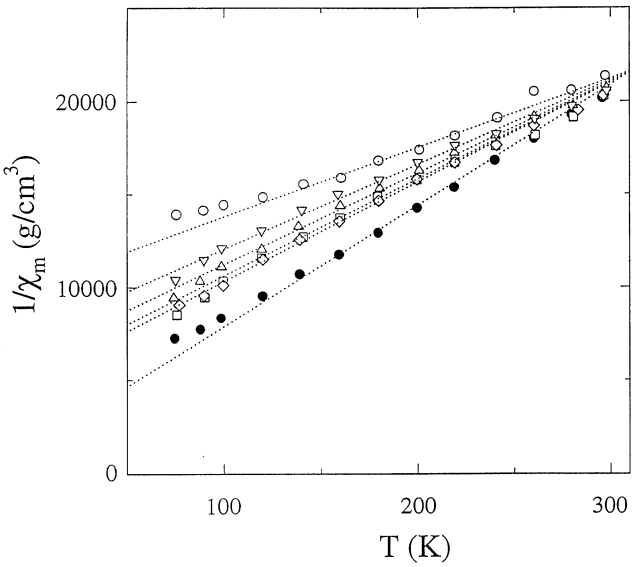

FIG. 7. Temperature dependence of the reciprocal magnetic mass susceptibility (χ_m^{-1}) for $x = 0.33$ (○), 0.36 (▽), 0.40 (□), 0.44 (△), 0.53 (◇), and 0.67 (●) samples.

entropy S_T associated with the ions surrounding a given site was previously considered negligible (23, 24). We obtained a mean value $\alpha \cong -30\,\mu V/K$ as shown in Fig. 6.

The α value we observed is rather small with respect to that already reported (21) ($-158\,\mu V/K$), but is consistent with our composition data if we assume that c is the fraction of Mn^{3+} sites (sources of conduction electrons) with respect to the total number of Mn^{3+} and Mn^{4+} sites of the spinel phase and that $\beta = 1$ consistently with the only available electronic configuration of high spin Mn^{3+} with non-degenerate e_g orbital states. From [1] we deduce $c \cong 0.42$ in good agreement with our composition data of Table 1. From these values we find that the c value ranges between 0.5 and 0.32 for samples with $0.33 \leq x \leq 0.40$, where the amount of the Li_2MnO_3 insulating phase is very low. This also matches the conductivity data. In fact, for a hopping conductivity

$$\sigma = \frac{A}{T}\exp\left(-\frac{E_H}{kT}\right), \qquad [2]$$

TABLE 3
Magnetic Moments and Weiss Constants

x	$m_{exp}(\mu_B)$	$m_{calc}(\mu_B)$	θ(K)
0.33	4.30	4.42	−251
0.36	4.35	4.29	−220
0.40	4.07	4.23	−146
0.44	4.09	4.17	−156
0.53	4.05	4.07	−119
0.67	3.91	3.87	−34

where E_H is the activation energy connected with the hopping mobility (22) and

$$A = \frac{NPc(1-c)e^2a^2v_0}{k}. \qquad [3]$$

Here v_0 represents the phonon frequency, a the lattice parameter, and P a probability factor for the electron transfer. For $0.33 \leq x \leq 0.40$, the $c(1-c)$ values range between 0.25 and 0.22 and the conductivity also exhibits nearly identical values. In contrast, for higher lithium content σ decreases, owing to the increase of the insulating Li_2MnO_3 phase amount.

Moreover, our compositional model is also consistent with the magnetic results if we suppose that the Mn^{3+} ions are in high spin ($S = 2$) configuration. Really, the calculated magnetic moments (m_{calc}) per Mn ion, as deduced from the sample compositions and assuming $m_{calc} = 4.90$ and $3.87\,\mu_B$ for Mn^{3+} and Mn^{4+}, respectively, well cover the experimental range (see Table 3). The data also agree with a recent study (7), differently from the data of Schutte *et al.* calling for the coexistence of high and low spin Mn^{3+} configurations (21).

Let us now comment on the temperature dependence of the χ_m we observed as a function of the Li content. All the investigated samples follow a typical Curie–Weiss law of antiferromagnetic materials. The θ values reported in Table 3 match those reported in (7) at least for $x \leq 0.40$. At larger x values, the relevant presence of the Li_2MnO_3 phase lowers our data approaching the θ value of the pure monoclinic compound. Nevertheless, deviations from the Curie–Weiss behavior were observed at lower temperature in the pure spinel compound (25), suggesting the presence of more complex magnetic properties.

It is interesting to note that the small anomaly in the linear dependence we observed in the $1/\chi_m$ curve around room temperature (Fig. 5b) follows analogous conductivity features in the same temperature range (Fig. 5a), corresponding to the presence of a structural transition already observed (10, 26). This transition was attributed to the Jahn–Teller effect on the octahedral coordination of the Mn^{3+} ions. The further addition of Li lowers the local symmetry and a weaker Jahn–Teller effect is expected for $x > 0.33$, in agreement with the χ_m and σ results in the other investigated samples.

5. CONCLUSIONS

A satisfactory correlation exists between the electrical properties of these Li–Mn mixed oxides and the coexisting phases compositional model we already proposed (9), resulting in the hopping conducting spinel and Li-rich phases and in the insulating Li_2MnO_3 monoclinic phase. The spinel

phase is a hopping electronic conductor in which the electron can move between adjacent Mn sites. The value of the ratio $Mn^{3+}/Mn^{4+} = 1$ in stoichiometric $LiMn_2O_4$ decreases in Li-rich samples as a consequence of the partial Li substitution in Mn octahedral sites. The activation energy (E_H) of the hopping process and the conductivity of the samples remain substantially constant in a quite large composition range ($0.33 \leq x \leq 0.40$). For $x > 0.40$ the conductivity decreases because of the relevant amount of Li_2MnO_3 insulating phase increasing with x.

The behavior of the static magnetic susceptibility in the paramagnetic region is also consistent with the Mn^{4+} and high spin Mn^{3+} ions concentration deduced from the sample composition, according to the results of a recent study (7).

The occurrence of Jahn–Teller effects suggests that the stoichiometric and nearly stoichiometric ($y < 0.04$) spinel is a single-phase compound. For higher Li content the spinel is not properly a single phase but a collection of phases with different composition and different lattice parameters. However, to achieve a reliable explanation of the XRD pattern characteristics, two limiting spinel phases have been considered, in addition to the diffraction effects pertinent to the Li_2MnO_3 phase, as discussed in Section 3.1.

For what concerns the evidence of anisotropic microstructural features in nearly stoichiometric spinel samples, a direct influence of the incipient cubic–tetragonal transition near room temperature may be inferred. A complete check of such a hypothesis on the basis of a microstructural study will be the subject of a further work.

ACKNOWLEDGMENTS

The work has been partially funded by CSGI. Helpful discussion with Paolo Scardi and Norberto Masciocchi about the application of simultaneous structure and size-strain parameter refinement, by the Rietveld method, is gratefully acknowledged.

REFERENCES

1. P. Barboux, J. M. Tarascon, and F. K. Shokoohi, *J. Solid State Chem.* **94,** 185 (1991).
2. J. M. Tarascon, W. R. McKinnon, F. Coowar, T. N. Bowmer, G. Amatucci, and D. Guyomard, *J. Electrochem. Soc.* **141,** 1421 (1994).
3. J. C. Hunter, *J. Solid State Chem.* **39,** 142 (1981).
4. M. M. Thackeray, P. J. Johnson, L. A. de Picciotto, P. G. Bruce, and J. B. Goodenough, *Mater. Res. Bull.* **19,** 179 (1984).
5. G. Pistoia, G. Wang, and C. Wang, *Solid State Ionics* **58,** 285 (1992).
6. G. A. Martin, A. Bates, V. Ducarme, and C. Mirodatos, *Appl. Catal.* **47,** 289 (1989).
7. C. Masquelier, M. Tabuchi, K. Ado, R. Kanno, Y. Kobayashi, Y. Macki, O. Nakamura, and J. B. Goodenough, *J. Solid State Chem.* **123,** 255 (1996).
8. V. Massarotti, M. Bini, and D. Capsoni, *Z. Naturforsch. A* **51,** 267 (1996).
9. V. Massarotti, D. Capsoni, M. Bini, C. B. Azzoni, and A. Paleari, *J. Solid State Chem.* **128,** 80 (1997).
10. A. Yamada, *J. Solid State Chem.* **122,** 160 (1996).
11. K. R. Morgan, S. Collier, G. Burns, and K. Ooi, *J. Chem. Soc., Chem Commun.* 1719 (1994).
12. H. M. Rietveld, *J. Appl. Crystallogr.* **2,** 65 (1969).
13. J. Schneider, "Proceeding IUCR Int. Workshop on the Rietveld Method, Petten" 1989.
14. D. B. Wiles and R. A. Young, *J. Appl. Crystallogr.* **14,** 149 (1981).
15. V. Massarotti, D. Capsoni, and M. Bini, *Z. Naturforsch. A* **50,** 155 (1995).
16. L. Lutterotti and P. Scardi, *J. Appl. Crystallogr.* **23,** 246 (1990).
17. G. Chiodelli and P. Lupotto, *J. Electrochem. Soc.* **138,** 9, 2703 (1991).
18. G. Chiodelli, G. Flor, and M. Scagliotti, *Solid State Ionics* **91,** 109 (1996).
19. D. G. Wickham and W. J. Croft, *J. Phys. Chem. Solids* **7,** 351 (1958).
20. P. Strobel and B. Lambert-Andron, *J. Solid State Chem.* **75,** 90 (1988).
21. L. Schutte, G. Colsman, and B. Reuter, *J. Solid State Chem.* **27,** 227 (1979).
22. H. L. Tuller and A. S. Nowick, *J. Phys. Chem. Solids* **38,** 859 (1977).
23. I. G. Austin and N. F. Mott, Adv. Phys. **18,** 41 (1969).
24. J. B. Goodenough, *Mater. Res. Bull.* **5,** 621 (1970).
25. N. Kumagai, T. Fujiwara, K. Tanno, and T. Horiba, *J. Electrochem. Soc.* **143**(3), 1007 (1996).
26. J. Sugiyama, T. Tamura, and H. Yamauchi, *J. Phys. Condens. Matter* **7,** 9755 (1995).